Available online at www.sciencedirect.com
SCIENCE DIRECT®
Journal of Computational Physics 203 (2005) 154–175
JOURNAL OF COMPUTATIONAL PHYSICS
www.elsevier.com/locate/jcp

# Interface pressure calculation based on conservation of momentum for front capturing methods

E. Shirani [1], N. Ashgriz *, J. Mostaghimi

*Department of Mechanical and Industrial Engineering, University of Toronto, Toronto, Ontario, Canada M5S 3G8*

Received 13 March 2003; received in revised form 26 July 2004; accepted 16 August 2004
Available online 1 October 2004

**Abstract**

A new method for the calculation of interface pressure for front capturing methods is developed. This method is based on the calculation of the pressure force at each interfacial cell face using the exact pressure due to the portion of the cell face that is occupied by each fluid. Special formulations for the pressure in the interfacial cells are derived for different orientations of an interface. This method (referred to as pressure calculation based on the interface location (PCIL)) is applied to the time evolution of a two-dimensional initially stagnant liquid drop in a gas, as well as, a gas bubble in liquid (gravity effects are not considered). A two-fluid, PLIC-VOF method is used to simulate the flow numerically. Both the continuum surface force (CSF) and the continuum surface stress (CSS) methods are used. A wide range of Ohnesorge numbers and density and viscosity ratios of two fluids are tested. It is shown that the new method reduces the spurious currents by up to three orders of magnitude for the cases tested.


*Keywords:* Volume-of-fluid method; Two-phase flow; Continuum surface force; Continuum surface stress; Interface; Pressure calculation based on interface location; PCIL; Free surface flows; Spurious currents; Parasitic currents

## 1. Introduction

In simulation of interfacial flows with fixed mesh, determination of the interface pressure and surface tension has been one of the most troublesome and challenging issues. Surface tension forces appear in equations by imposing a jump condition across the interface. This condition is difficult to apply numerically and has been the center of attention by many researchers.

* Corresponding author. Tel.: +1 416 946 3408; fax: +1 416 978 7753.
*E-mail address:* ashgriz@mie.utoronto.ca (N. Ashgriz).
[1] Permanent address: Department of Mechanical Engineering, Isfahan University of Technology, Isfahan, Iran.

0021-9991/$ - see front matter 
doi:10.1016/j.jcp.2004.08.017

Surface tension may be implemented by one of the following two methods. One is by applying the surface tension as a boundary condition along the free surface. For a staggered fixed mesh, an interpolation scheme is used to ensure that the computed surface pressure is correct in relation to the cell-centered pressure. If it is not, the solution is iterated until the final pressure field is within some tolerance value of the previous iteration. If it is, the correct pressure solution is obtained, and the overall Navier–Stokes solution is advanced to the next time level. This technique is not popular for two reasons. First, the cost of multiple iterations at each time-step is high. In most cases, the time-step restrictions, which would ensure stability, require very small values. Therefore, these additional iterations at each time-step would increase the overall computational time needed to obtain a solution. Secondly, in order to properly implement this method, the exact location of the free surface at the next time step is required. Although the interface location can be determined through various methods (i.e., using VOF [1–15] or level set reconstruction techniques [16]), its value is only known at the existing time-level, and not at the next-time level.

In order to circumvent the problems associated with the pressure calculation at the exact interface boundary, Brackbill et al. [17] have developed a method referred to as the continuum surface force (CSF) method. This method replaces the need to know the exact location of the free surface by converting the surface tension forces into an equivalent volume force, which is added to the Navier–Stokes equations as an additional body force. This force has smoothed properties and acts only in a finite transition region across the interface. Note that the transition region is the region which contains the interfacial cells and their immediate neighboring cells. The CSF model reformulates surface tension into an equivalent volume force $F^{\mathrm{st}}$ as follows:

$$F^{\mathrm{st}}(x) = \sigma \int_S \kappa \mathbf{n} \delta(\mathbf{x} - \mathbf{x}_s)\, \mathrm{d}S, \tag{1}$$

where $\sigma$ is the surface tension coefficient, $\kappa$ is the surface curvature, $\mathbf{n}$ is the unit normal to the surface in the outward direction, $\delta(\mathbf{x} - \mathbf{x}_s)$ is the Dirac delta function, and $\mathbf{x}_s$ are points on the interface $S$. Surface tension is then incorporated into the flow equations simply as a component of the body force.

The original discretization of $F^{\mathrm{st}}$ proposed by Brackbill et al. [17] led to the formation of artificial velocities (the so-called "spurious" or "parasitic" currents) due to an inaccurate representation of surface tension terms and associated pressure jump. These currents are strongly growing vortical flows in the transition region. In a paper by Brackbill and Kothe [18], they showed that the original CSF formulation produces a vorticity source term and concluded that these currents will disappear as the transition region approaches zero. In an effort to reduce these effects, Aleinov and Puckett [19] suggested another formulation of $F^{\mathrm{st}}$, which has been adopted by Bussmann et al. [20]. In their formulation, first, the surface force per unit volume is computed within each of the interface cells and it is placed at the center of the cell:

$$F^{\mathrm{st}}_{i,j,k} = \sigma \kappa_{i,j,k} \frac{A_{i,j,k}}{v_{i,j,k}} n_{i,j,k}, \tag{2}$$

where $A_{i,j,k}$ is the surface area of the fluid contained within the cell and $v_{i,j,k}$ is the cell volume. This force is then smoothed by convolving it with a smoothing kernel, $K$:

$$\tilde{F}^{\mathrm{st}}_{i,j,k} = K F^{\mathrm{st}}_{i,j,k}. \tag{3}$$

Significant effort has been made to improve the surface tension force predictions by using higher order kernels for more accurate estimations of the curvature, $\kappa$, and the unit normal vector, $\mathbf{n}$, to the interface. In the original CSF method [17], the kernel is a quadratic $B$-spline. There are several other Kernels [21–23], but the most widely used smoothing kernel is that proposed by Peskin [24]. Lafaurie et al. [25] developed a new

method referred to as the continuum surface stress, CSS, method, in which they converted the volumetric force used in the CSF method into a stress term. In the CSS model, capillary force are represented as a stress tensor $\mathbf{T}$, which is tangential to the interface and it is given by

$$\mathbf{T} = -\sigma(\mathbf{I} - \mathbf{n} \otimes \mathbf{n})\delta_S, \tag{4}$$

where $\mathbf{I}$ is the unit tensor $\delta_{ij}$ and $\delta_S$ is a delta function. Then the capillary force is written as:

$$\mathbf{F}^{\mathrm{st}} = -\nabla \cdot \mathbf{T}. \tag{5}$$

The CSS method also produces numerical spurious effects [25]. In fact, neither CSF nor CSS models produce very accurate solution in capillary dominated fluid problems. In problems where the surface tension forces dominate the viscous forces, the spurious currents can cause interface oscillations and deform or destroy the interface.

Popinet and Zaleski [26] have reduced the spurious currents considerably by using a Lagrangian advection marker to advect the interface. The pressure is calculated based on the location of the interface at each cell face. Two values for the pressure at each interfacial cell face are determined using the pressure at the two neighboring cells. A new source term is added to the Poisson equation to accurately calculate the pressure. Their method resulted in a more accurate calculation of the surface tension force and the associated pressure jump [26]. Their work, however, is currently limited to the markers method. Meier et al. [27] have also developed a new method to reduce the spurious currents. Their method is based on improving the curvature calculation. They have used an estimator function, which is tuned with a least-squares-fit against the reference data. They have indicated that their method is 3–7 times more accurate than the CSF method of Brackbill, etc. [17]. They have been able to reduce the intensity of the spurious currents by up to 100 times. Although their method calculates the interface curvature more accurately, the pressure force at each cell face is still poorly calculated. This will be further discussed later in this paper. Renardy and Renardy [28] have introduced PROST, a VOF-based algorithm, which uses a least-square fit to the volume fractions to determine the interface properties. Their model significantly reduces the spurious currents, even without any smoothing of the volume fractions. Jamet et al. [29] used a second-gradient method to reduce the truncation error in the computation of the energy exchanges between the surface and the kinetic energies. By ensuring energy conservation, the parasitic currents were reduced drastically.

Although the above methods reduce the spurious currents by some orders of magnitude, the methods are expensive, somewhat complicated and they may not accurately calculate the pressure force at the interface. Here, we present a new method, which we refer to as the pressure calculation based on the interface location (PCIL). We will show that by an accurate implementation of the pressure forces at the interface cells, it is possible to eliminate a significant portion of the spurious currents. By using this new method the spurious currents can be reduced by up to three orders of magnitude. Unlike the above-mentioned methods, PCIL model is simple and extremely inexpensive (very limited extra calculations are needed to implement PCIL model). The new method is directly derived by applying the momentum balance on each interface cell. The derivations and relations given in this paper are for two-dimensional problems, however, the method can be extended to three-dimensional cases. In the next section, we will present the problem formulation, followed by our method for the calculation of the interface pressures. The new method is then tested on the time evolution of initially stationary drops and bubbles.

## 2. Problem formulation

We will solve the unsteady, incompressible Navier–Stokes equations in two dimensions for two fluids with interfaces. A volume-of-fluid, VOF, method along with a piecewise linear interface calculation, PLIC, is used to capture the fluid interfaces. It is assumed that the velocity field is continuous across the interface,

but there is a pressure jump at the interface due to the presence of the surface tension. The governing equations describing this problem are:

$$\frac{\partial u_i}{\partial x_i} = 0, \tag{6}$$

$$\frac{\partial F}{\partial t} + u_i \frac{\partial F}{\partial x_i} = 0 \tag{7}$$

and

$$\frac{\partial \rho u_i}{\partial t} + \frac{\partial \rho u_i u_j}{\partial x_j} = -\frac{\partial p}{\partial x_i} + F^{\mathrm{st}} \cdot \hat{i} + \mu \frac{\partial^2 u_i}{\partial x_j^2} + \rho g_i, \tag{8}$$

where $u_i$s are the velocity components, and $t$ and $x_i$ are time and space coordinates. $F$ is the volume fraction of the fluid, which is zero where only fluid 2 exists and is one where only fluid 1 exits. $p$ is the pressure, $\hat{i}$ is the unit vector in the $i$th direction and $\rho$ and $\mu$ are the fluid density and absolute viscosity, respectively, and they depend on the densities and viscosities of each fluid as:

$$\rho = \rho_2 + F(\rho_1 - \rho_2) \tag{9}$$

and

$$\mu = \mu_2 + F(\mu_1 - \mu_2), \tag{10}$$

where $\rho_1$ and $\rho_2$, $\mu_1$ and $\mu_2$ are densities and viscosities of fluids 1 and 2, respectively. In addition, the following Poisson equation needs to be solved:

$$\frac{\partial}{\partial x_i}\left(\frac{\partial p}{\partial x_i}\right) = -\frac{\partial}{\partial x_i}\left[\frac{\partial}{\partial x_j}(\rho u_i u_j - 2\mu S_{ij})\right], \tag{11}$$

where $S_{ij}$ is the rate of strain tensor.

## 3. Formulation of the pressure at the interface

Consider a two-dimensional interface cell shown in Fig. 1, in which fluid 1 and 2 are separated by an interface line. We denote fluid 1 as the heavier fluid and fluid 2 as the lighter fluid throughout this paper. If the surface tension forces are considered, then there would be a pressure jump at the interface, and the two fluids will have different pressures.

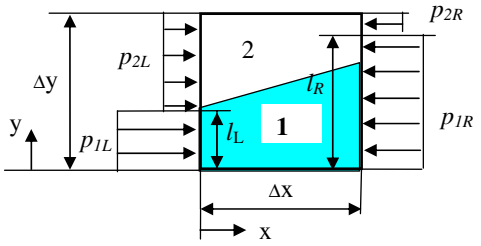


Fig. 1. An interface cell with cell face pressures along the $x$-axis.

In order to calculate the pressure force exerted on the cells, we will apply the momentum balance to each cell. Consider the pressure force acting along the $x$-direction on the cell in Fig. 1. The pressure force per unit area on the left side of the cell is, $F_{p\mathrm{L}}$:

$$F_{p\mathrm{L}} = \frac{p_{\mathrm{L}}\Delta y}{\Delta y} = p_{1\mathrm{L}}\frac{l_{\mathrm{L}}}{\Delta y} + \frac{\Delta y - l_{\mathrm{L}}}{\Delta y}p_{2\mathrm{L}} \tag{12}$$

or

$$F_{p\mathrm{L}} = p_{\mathrm{L}} = p_{1\mathrm{L}}H_{\mathrm{L}} + (1 - H_{\mathrm{L}})p_{2\mathrm{L}}, \tag{13}$$

where $p_{\mathrm{L}}$ is the average pressure on the left side, $\Delta y$ is the length of the cell in the $y$-direction, $l_{\mathrm{L}}$ is the length of the cell side which is in contact with fluid 1, and $H_{\mathrm{L}} \equiv (l_{\mathrm{L}}/\Delta y)$. Eq. (13) may be rearranged as:

$$p_{\mathrm{L}} = p_{2\mathrm{L}} + H_{\mathrm{L}}(p_{1\mathrm{L}} - p_{2\mathrm{L}}). \tag{14}$$

The pressure difference in the parentheses represents the pressure jump due to the surface tension. Similar relations can be obtained for the pressure force on the right (R), top (T) and bottom (B) sides:

$$p_{\mathrm{R}} = p_{2\mathrm{R}} + H_{\mathrm{R}}(p_{1\mathrm{R}} - p_{2\mathrm{R}}), \tag{15}$$

$$p_{\mathrm{T}} = p_{2\mathrm{T}} + H_{\mathrm{T}}(p_{1\mathrm{T}} - p_{2\mathrm{T}}) \tag{16}$$

and

$$p_{\mathrm{B}} = p_{2\mathrm{B}} + H_{\mathrm{B}}(p_{1\mathrm{B}} - p_{2\mathrm{B}}) \tag{17}$$

or in general,

$$p_k = p_{2k} + H_k(p_{1k} - p_{2k}), \tag{18}$$

where $H_k$ ($k$ = L, R, T, B) is a non-dimensional parameter that denotes the location of the interface at cell side $k$. The value of $H_k$ is equal to the relative height (area in 3-D) of a cell side $k$, which is in contact with fluid 1. The value of $H_k$ is between zero and one in the interface cells and it is one or zero in the full cells, depending on being in fluid 1 or 2, respectively. Note that the value of $H_k$ depends on the amount of the fluid 1 or 2, as well as, the interface orientation. The previous interface capturing methods have not considered $H_k$ in their calculation of pressure force. Based on our model, this means that the previous methods have assumed that $H_k = 1$ everywhere. The above analysis shows that this assumption can be a source of error, especially in the cells with relatively large fraction of the lighter fluid (fluid 2), where the value of $H_k$ is small.

For cell faces which are in contact only with fluid 1, $H(H_k) = 1$ and $p = p_1$. For cell faces which are in contact only with fluid 2, $H(H_k) = 0$ and $p = p_2$. For cell faces which are in contact with both fluids, $0 < H(H_k) < 1$ and $p$ is between $p_1$ and $p_2$.

Similar results can be obtained in a three-dimensional system, where $H_k$ becomes the ratio of the cell side "area" that is in contact with fluid 1 to the whole cell side "area". Eqs. (14)–(18) are held for the three-dimensional case as well, except that there will be six different $H_k$s, one for each cell face.

The pressure jump, $p_s$, at any interface point is related to the surface tension coefficient according to:

$$p_s = p_1 - p_2 = \sigma\kappa, \tag{19}$$

where $\kappa$ is the interface curvature. Therefore, Eq. (18) becomes:

$$p_k = p_{2k} + H_k\sigma\kappa, \tag{20}$$

and the pressure force per unit area, $F_{pk}$, acting on an interfacial cell side, $k$, is obtained from Eqs. (13) and (20):

$$F_{pk} = p_{2k} + H_k\sigma\kappa. \tag{21}$$

The second term in the right-hand side of Eq. (21) is the normal force per unit area due to the pressure jump or surface tension force,

$$\mathbf{F}_s^{\mathrm{st}} = H\sigma\kappa\mathbf{n}. \tag{22}$$

Following Brackbill et al.'s [17] continuum surface force (CSF) model, the interface curvature and the surface tension may be calculated as:

$$\kappa(\mathbf{x}) = -\nabla\cdot\tilde{\mathbf{n}}(\mathbf{x}) = \nabla\cdot\frac{\nabla\tilde{F}(\mathbf{x})}{|\nabla\tilde{F}(\mathbf{x})|} \tag{23}$$

and

$$F_v^{\mathrm{st}} = \sigma\kappa\delta_s\mathbf{n} = \sigma\kappa\mathbf{n}\frac{|\nabla\tilde{F}|}{[F]}, \tag{24}$$

where the $\sim$ (tilda) denotes filtered (smoothed) value, the square brackets denote the difference between the maximum and the minimum values of the function inside the brackets, and $F_v^{\mathrm{st}}$ is the volumectric surface tension force. The above model produces an artificial acceleration in the lighter fluid when the density ratio of the two fluids is large. This acceleration is the main source of producing spurious currents. Brackbill et al. [17,30] recommended addition of a density scaling factor in order to reduce the formation of such acceleration. Therefore, they proposed the following equation instead of Eq. (24):

$$F_v^{\mathrm{st}} = \sigma\kappa\delta_s\mathbf{n} = \sigma\kappa\mathbf{n}\frac{|\nabla\tilde{F}|}{[F]}\frac{\rho(x)}{[\rho]}, \tag{25}$$

where $\rho(x)$ is the local value of the density obtained by Eq. (9) and $[\rho]$ is the difference between the density of the heavier and the lighter fluids. The density correction term (the second fraction in Eq. (25)) is added to correct the force in the momentum equation. This dampens the acceleration of the lighter fluid in the cells near the interface that contain small amounts of heavier fluid. The newly added fraction is not directly obtained from any conservation law, but it is only postulated. We will later examine the effectiveness of this term and will compare it with our PCIL model. The volumetric surface force, defined in Eq. (24), based on our PCIL model (using Eq. (20)) becomes:

$$F_v^{\mathrm{st}} = H\sigma\kappa\delta_s\mathbf{n} = H\sigma\kappa\mathbf{n}\frac{|\nabla\tilde{F}|}{[F]}. \tag{26}$$

We will use this equation to compare our results with those of Eq. (25).

Another model, which is widely used, is that of Zaleski's continuous surface stress (CSS) model [25,31–33]. In this model, Eq. (25) is replaced with:

$$F_v^{\mathrm{st}} = \sigma\kappa\delta_s\mathbf{n} = \sigma\nabla\cdot\left(|\nabla F|\mathbf{I} - \frac{\nabla F\otimes\nabla F}{|\nabla F|}\right). \tag{27}$$

Again, using our PCIL model, the CSS model becomes:

$$F_v^{\mathrm{st}} = H\sigma\kappa\delta_s\mathbf{n} = H\sigma\nabla\cdot\left(|\nabla F|\mathbf{I} - \frac{\nabla F\otimes\nabla F}{|\nabla F|}\right). \tag{28}$$

We will compare the results of each of these models in the later sections. Note that in this paper the filtered value of volume fraction, $\tilde{F}$, is used for the CSF model, whereas $F$ is not filtered for the CSS model. This is because, based on our experience, unfiltered values of $F$ used in the CSF model result in inaccurate calculation of the surface tension forces. However, this is not the case for the CSS model. For simplicity, from now on, we drop the superscript tilda in the formulas.

## 4. Calculation of the interface function $H_k$

Consider a two-dimensional cell. In the piecewise linear interface calculation (PLIC) method, the interface is approximated by a straight line of an appropriate inclination in each cell. The straight lines are not connected to each other at the cell faces. That is, the interface line at each cell is determined independent of the neighboring interface lines, and their ends need not necessarily be connected at the cell faces. Each line is determined so that it is perpendicular to an interface normal vector, and it divides the cell surface into two regions that match the given $F$ for the cell (see [8] for details). The interface normal vector $\mathbf{n}$ (a unit vector perpendicular to the interface pointing to fluid 2) for each cell is determined using the gradient of $F$:

$$\mathbf{n} = -\frac{\nabla F}{|\nabla F|}, \tag{29}$$

where the gradient of $F$ at each point is calculated using the values of $F$ in its immediate nine neighboring points. Assuming $\Delta x = \Delta y = h$, the $x$ and the $y$ components of the gradient of $F_{i,j}$ are:

$$m_{x,i,j} = \lfloor F_{i+1,j+1} - F_{i-1,j+1} + 2(F_{i+1,j} - F_{i-1,j}) + F_{i+1,j-1} - F_{i-1,j-1} \rfloor / h \tag{30}$$

and

$$m_{y,i,j} = \lfloor F_{i+1,j+1} - F_{i+1,j-1} + 2(F_{i,j+1} - F_{i,j-1}) + F_{i-1,j+1} - F_{i-1,j-1} \rfloor / h. \tag{31}$$

And the $x$ and the $y$ components of the unit normal vector are:

$$n_{x,i,j} = -\frac{m_{x,i,j}}{\sqrt{m_{x,i,j}^2 + m_{y,i,j}^2}} \tag{32}$$

and

$$n_{y,i,j} = -\frac{m_{y,i,j}}{\sqrt{m_{x,i,j}^2 + m_{y,i,j}^2}}, \tag{33}$$

where $n_x$ and $n_y$ are the components of $\mathbf{n}$. Once the normalized unit vector $\mathbf{n}$ is calculated, a straight line is positioned perpendicular to it in such a way that it matches the value of $F$ in the cell.

Fig. 2 shows that depending on the orientation of the interface, eight different cases may occur. The normal vector angle, $\theta$, (shown in Fig. 3) can take any value between zero and $2\pi$. We have obtained the relation for $H$ for the case when $\mathbf{n}$ is in the first octant ($0 \leqslant \theta \leqslant \pi/4$). By mirroring appropriately on the $x$ and $y$ axes, and the bisector between them, equivalent situations are obtained when $\mathbf{n}$ is in the other octants. Figs. 2 and 3 show that the area filled with fluid 1 can be triangle, quadrilateral or pentagon, depending on the values of $F$, $n_x$ and $n_y$ in the cell. The limiting values of $F$ for the cases when $\mathbf{n}$ is in the first octant and $n_x > n_y$, are:

$$F_{\lim,1} = \frac{n_y}{2n_x} \quad \text{and} \quad F_{\lim,2} = 1 - F_{\lim,1}. \tag{34}$$

For a general case, where $\mathbf{n}$ is arbitrary, the limiting values may be calculated as:

$$F_{\lim,1} = \frac{n_{\min}}{2n_{\max}} \quad \text{and} \quad F_{\lim,2} = 1 - F_{\lim,1}, \tag{35}$$

where

$$n_{\min} = \min(|n_x|, |n_y|) \quad \text{and} \quad n_{\max} = \max(|n_x|, |n_y|). \tag{36}$$

In order to calculate $H_k$ on each side of a cell, the locations of $a$ and $b$, the two ends of the straight line in each cell need to be determined. $a$ and $b$ are determined such that the cross product $\mathbf{n} \times \overrightarrow{ab}$ is positive. Note that if the length of the cell sides are equal to one, then the values of $H_k$s are equal to $a$ and $b$. Therefore, $H_k$

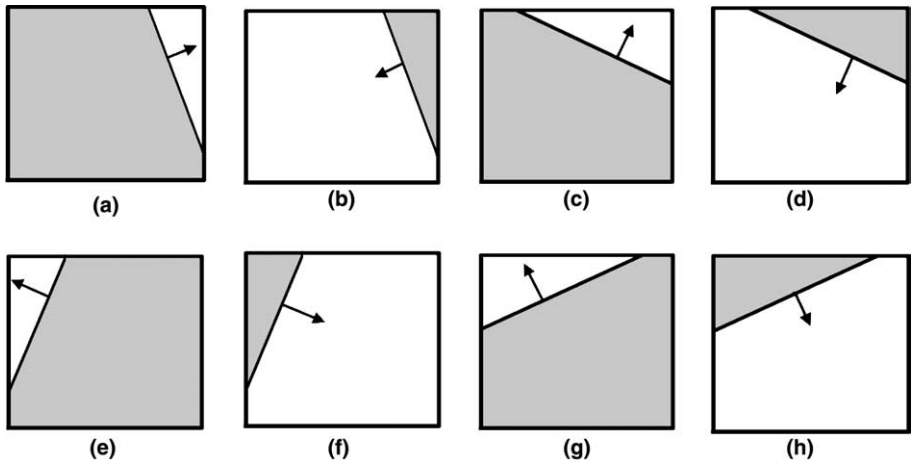


Fig. 2. Different interface configurations. The shaded area represents fluid 1 and the blank area represents fluid 2. (a) $|n_x| \geqslant |n_y|$, $n_x > 0$, $n_y \geqslant 0$ (b) $|n_x| \geqslant |n_y|$, $n_x < 0$, $n_y \leqslant 0$ (c) $|n_y| > |n_x|$, $n_x > 0$, $n_y \geqslant 0$ (d) $|n_y| > |n_x|$, $n_x < 0$, $n_y \leqslant 0$ (e) $|n_x| \geqslant |n_y|$, $n_x < 0$, $n_y \geqslant 0$ (f) $|n_x| \geqslant |n_y|$, $n_x > 0$, $n_y \leqslant 0$ (g) $|n_y| > |n_x|$, $n_x < 0$, $n_y \geqslant 0$ (h) $|n_y| > |n_x|$, $n_x > 0$, $n_y \leqslant 0$.

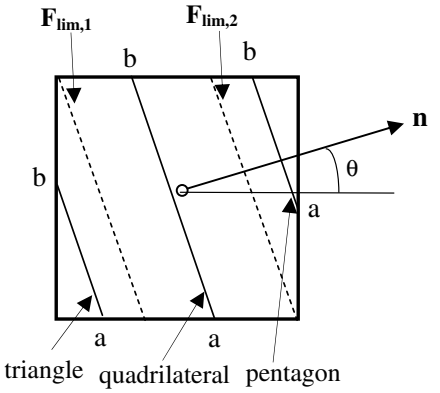


Fig. 3. Different interface configurations.

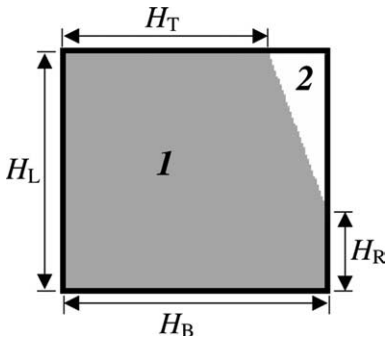


Fig. 4. A cell with normal in the first octant. The darker area is fluid 1. $H_k$s are shown for unit length cell.

for each cell face follows immediately from a first or a second order equation. For the case when **n** is in the first octant, let $H_k$s at the bottom, right, top and left sides of the cell be represented by $H_1$, $H_2$, $H_3$, and $H_4$, respectively (see Fig. 4). They can be described according to the following relations:

For $F \leqslant F_{\lim,1}$(triangle):

$$H_1 = \sqrt{2F\frac{n_{\min}}{n_{\max}}}, \quad H_2 = 0, \quad H_3 = 0, \quad H_4 = \frac{2F}{H_1}. \tag{37}$$

For $F_{\lim,1} < F \leqslant F_{\lim,2}$(quadrilateral):

$$H_1 = F + \frac{n_{\min}}{2n_{\max}}, \quad H_2 = 0, \quad H_3 = F - \frac{n_y}{2n_x}, \quad H_4 = 1. \tag{38}$$

For $F > F_{\lim,2}$(pentagon):

$$H_1 = 1, H_2 = 1 - \sqrt{2(1-F)\frac{n_{\max}}{n_{\min}}}, \quad H_3 = 1 - \frac{2(1-F)}{1-H_2}, \quad H_4 = 1. \tag{39}$$

Values of $H_k$s at the top, bottom, left and right sides of a cell, $H_T$, $H_B$, $H_L$, $H_R$, with an arbitrary interface normal vector are obtained from the above $H_1$, $H_2$, $H_3$, and $H_4$ by mirroring approximation. Depending on the local value of $F$, the values of $H_k$s are chosen from one of Eqs. 37. Fig. 2 shows all of the possible interface configurations. The results depend on the relative values of $n_x$ and $n_y$, and are given in Table 1. Note that the calculation of $H_k$ does not need extra operation in VOF method, since the values of $n_x$, $n_y$, $a$ and $b$ are already calculated during the interface reconstruction process.

Except for the cell faces at the boundaries of the computational domain, each cell face is adjacent to two of the other cells. Thus, two values are calculated for $H_k$, one from each of the interior cell faces.

Table 1
Values of $H$s at the cell faces corresponding to the configurations in Fig. 2

| $H$ values | Case | | | | | | | |
|---|---|---|---|---|---|---|---|---|
| | $n_x \geqslant 0$, $n_y > 0$ | | $n_x \leqslant 0$, $n_y > 0$ | | $n_x \leqslant 0$, $n_y < 0$ | | $n_x \geqslant 0$, $n_y < 0$ | |
| | $\lvert n_x\rvert \geqslant \lvert n_y\rvert$ | $\lvert n_y\rvert > \lvert n_x\rvert$ | $\lvert n_x\rvert \geqslant \lvert n_y\rvert$ | $\lvert n_y\rvert > \lvert n_x\rvert$ | $\lvert n_x\rvert \geqslant \lvert n_y\rvert$ | $\lvert n_y\rvert > \lvert n_x\rvert$ | $\lvert n_x\rvert \geqslant \lvert n_y\rvert$ | $\lvert n_y\rvert > \lvert n_x\rvert$ |
| $H_B$ | $H_1$ | $H_4$ | $H_1$ | $H_4$ | $H_3$ | $H_2$ | $H_3$ | $H_2$ |
| $H_R$ | $H_2$ | $H_3$ | $H_4$ | $H_1$ | $H_4$ | $H_1$ | $H_2$ | $H_3$ |
| $H_T$ | $H_3$ | $H_2$ | $H_3$ | $H_2$ | $H_1$ | $H_4$ | $H_1$ | $H_4$ |
| $H_L$ | $H_4$ | $H_1$ | $H_2$ | $H_3$ | $H_2$ | $H_3$ | $H_4$ | $H_1$ |

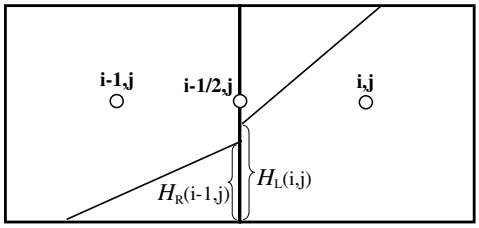


Fig. 5. Two adjacent cells with an interface.

For example, for the left side of the cell $i, j$, we have $H_{L,i,j}$, and for the right side of the cell $i-1, j$, we have $H_{R,i-1,j}$ (see Fig. 5). If the interface lines are not connected to each other, as shown in Fig. 5, the two values of $H_k$ may be different. Based on several different trials, we have found that a simple averaging method works well to eliminate this problem. That is:

$$H_{ki-1/2,j} = \tfrac{1}{2}(H_{Ri-1,j} + H_{Li,j}). \tag{40}$$

This prevents having internal pressure forces as source terms in the flow field. It is worth noting that for each side of the cell, one should use the corresponding value of $H_k$ for the same side (Eq. (40)). In other words, one cannot calculate one $H$ for the center of each cell and use it for all sides of the same cell.

The PCIL method explained above may be summarized by the following steps:

1. Determination of the intersection locations of an interface line with the cell faces.
2. Calculations of the non-dimensional parameter $H_k$, by normalizing the intersection locations with the cell face length.
3. Averaging the two values of $H_k$s obtained for both sides of each internal cell face, Eq. (40).
4. Multiplying the value of $H_k$ to the capillary forces used in the momentum equation, Eq. (26) or (28). Note that the $x$-momentum equation is applied at the cell faces perpendicular to the $x$-axis, at point $i-1/2, j$ shown in Fig. 5 and the $y$-momentum equation is applied at the cell faces perpendicular to the $y$-axis, at point $i, j-1/2$.

## 5. Results and discussions

We have tested the PCIL method on the temporal evolution of a two-dimensional liquid drop. A circular drop of a fluid in the absence of gravity is placed inside of a second fluid. The initial velocities of both fluids are set to zero. The drop radius, $r$, the fluid densities, $\rho_1$ and $\rho_2$, the viscosities, $\mu_1$ and $\mu_2$, and the surface tension coefficient, $\sigma$, are the main physical variables (subscript 1 stands for the drop and 2 for the surrounding fluid). The number of grid points, the time step, $\Delta t$, and the grid size, $h$, are the numerical

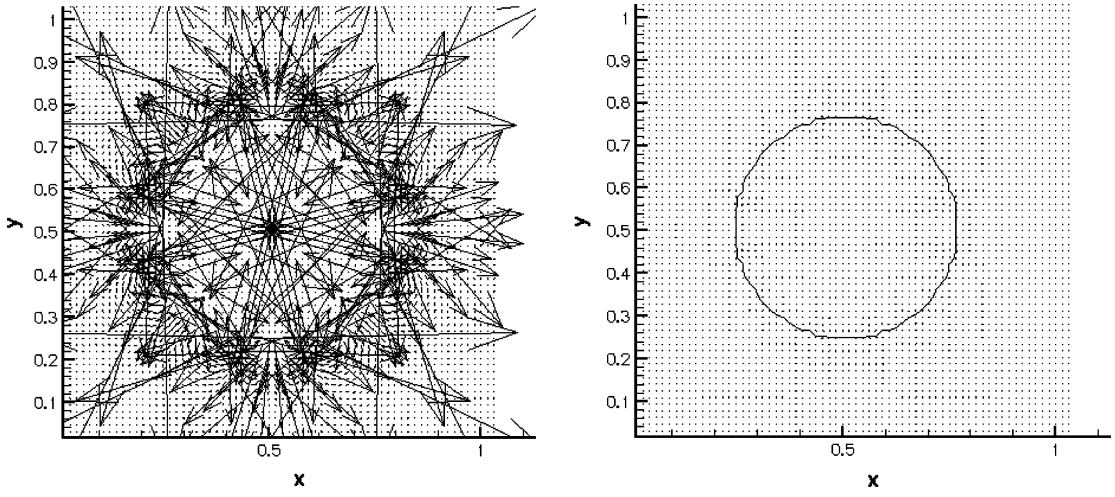


Fig. 6. Spurious currents with the same velocity scales, for CSS model without PCIL model (left) and with PCIL model (right).

parameters. The computational grid is fixed, rectangular and uniform. The code SURFER [25] is modified and used in this work. The details of the numerical method based on VOF-PLIC and Chorin's projection method for a semi-implicit Navier–Stokes solver, which have been used in this code, are given in [25,31,32] and are not repeated here. Two different continuum methods, namely the CSF [17] and the CSS [25] methods, for modeling the interfacial tension are used in this work. We have examined the performance of these methods with and without the PCIL model. Number of the grid points, the grid size, the time step, and the radius of the drop are held fixed. We will investigate the effects of variation of physical properties (i.e., density, viscosity and surface tension coefficient) on the flow field.

If the computed pressure gradient at the drop interface does not balance with the surface tension forces, spurious currents will be formed. These currents tend to grow with time. The spurious currents are also affected by the grid size as shown by Renardy and Renardy [28], and Meier et al. [27]. Therefore, the grid dependency has also been examined. The drop radius is taken as $0.25L$, where $L$ is the domain length in the

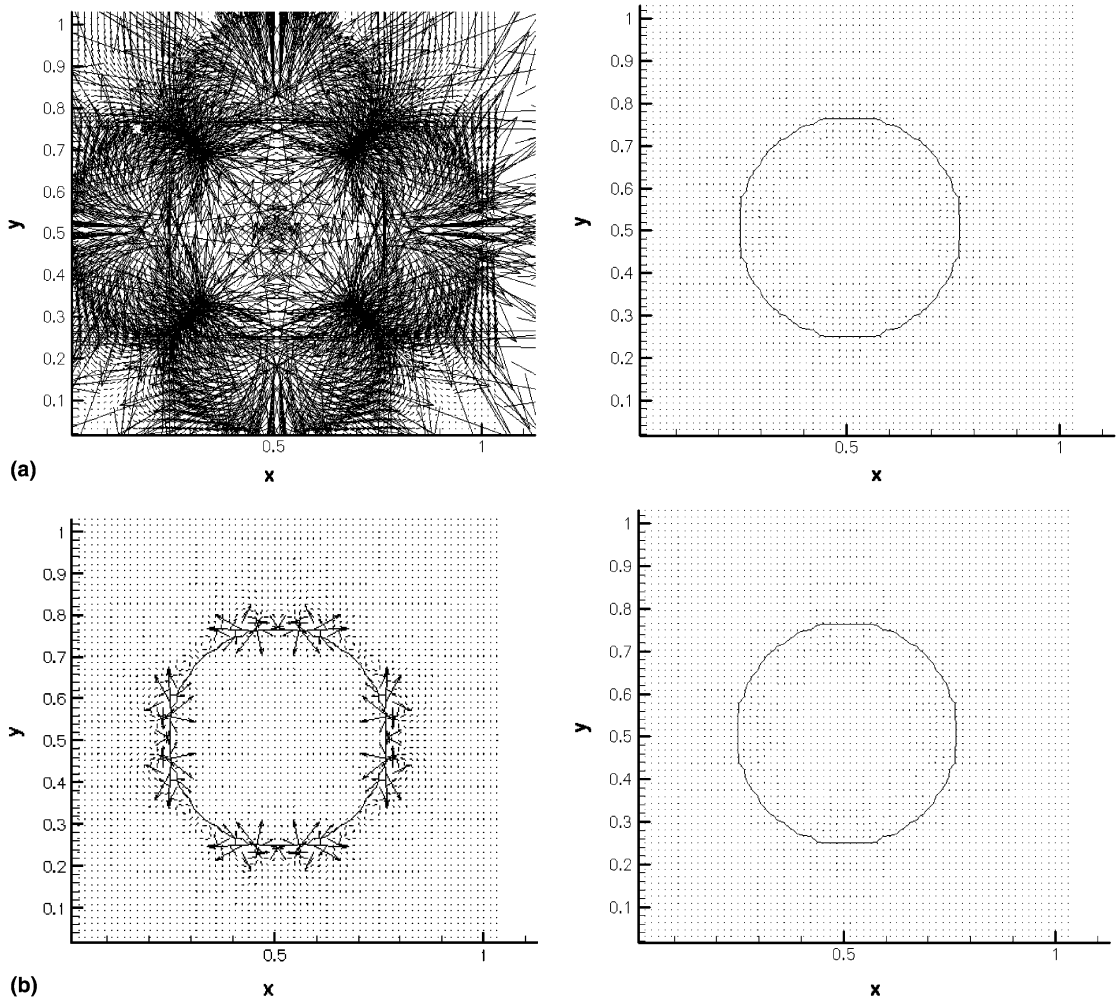


Fig. 7. Spurious currents (with the same velocity scales) using model (a) without and (b) with density modification. Figures on the left are without PCIL model and those on the right are with PCIL model.

Table 2
Values of the maximum and the norm velocities of spurious currents using CSS model

| Number of time steps | $V_{max}$ | | $V_{norm}$ | |
|---|---|---|---|---|
| | w/o PCIL | with PCIL | w/o PCIL | with PCIL |
| 1000 | 1.067e − 2 | 3.166e − 5 | 2.611e − 4 | 3.483e − 6 |
| 4000 | 4.162e − 2 | 1.261e − 4 | 1.032e − 3 | 1.393e − 5 |
| 8000 | 7.806e − 2 | 2.515e − 4 | 2.017e − 3 | 2.787e − 5 |

Table 3
Values of the maximum velocities of spurious currents for CSF model

| Number of time steps | Without density correction | | With density correction | |
|---|---|---|---|---|
| | w/o PCIL | with PCIL | w/o PCIL | with PCIL |
| 1000 | 3.619e − 2 | 3.273e − 5 | 1.482e − 3 | 3.118e − 5 |
| 4000 | 1.31e − 1 | 1.308e − 4 | 5.873e − 3 | 1.246e − 4 |
| 8000 | 2.31e − 1 | 2.610e − 4 | 1.155e − 2 | 2.488e − 4 |

Table 4
Values of the norm of the velocities of spurious currents for CSF model

| Number of time steps | Without density correction | | With density correction | |
|---|---|---|---|---|
| | w/o PCIL | with PCIL | w/o PCIL | with PCIL |
| 1000 | 1.421e − 3 | 4.286e − 6 | 2.043e − 5 | 3.486e − 6 |
| 4000 | 5.638e − 3 | 1.713e − 5 | 1.208e − 4 | 1.394e − 5 |
| 8000 | 1.103e − 2 | 3.422e − 5 | 2.391e − 4 | 2.785e − 5 |

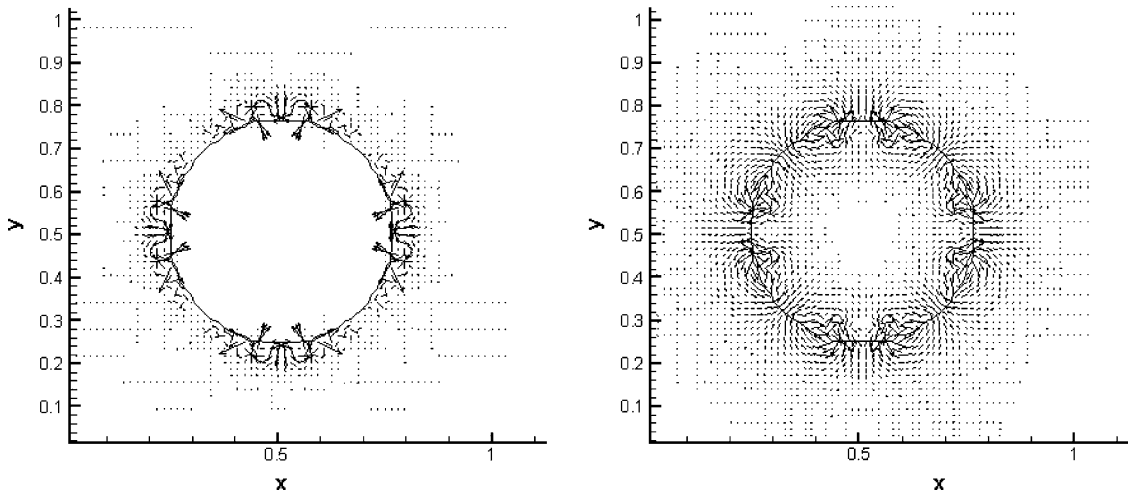


Fig. 8. Spurious currents with different velocity scales, for CSS model without PCIL model (left) and with PCIL model (right).

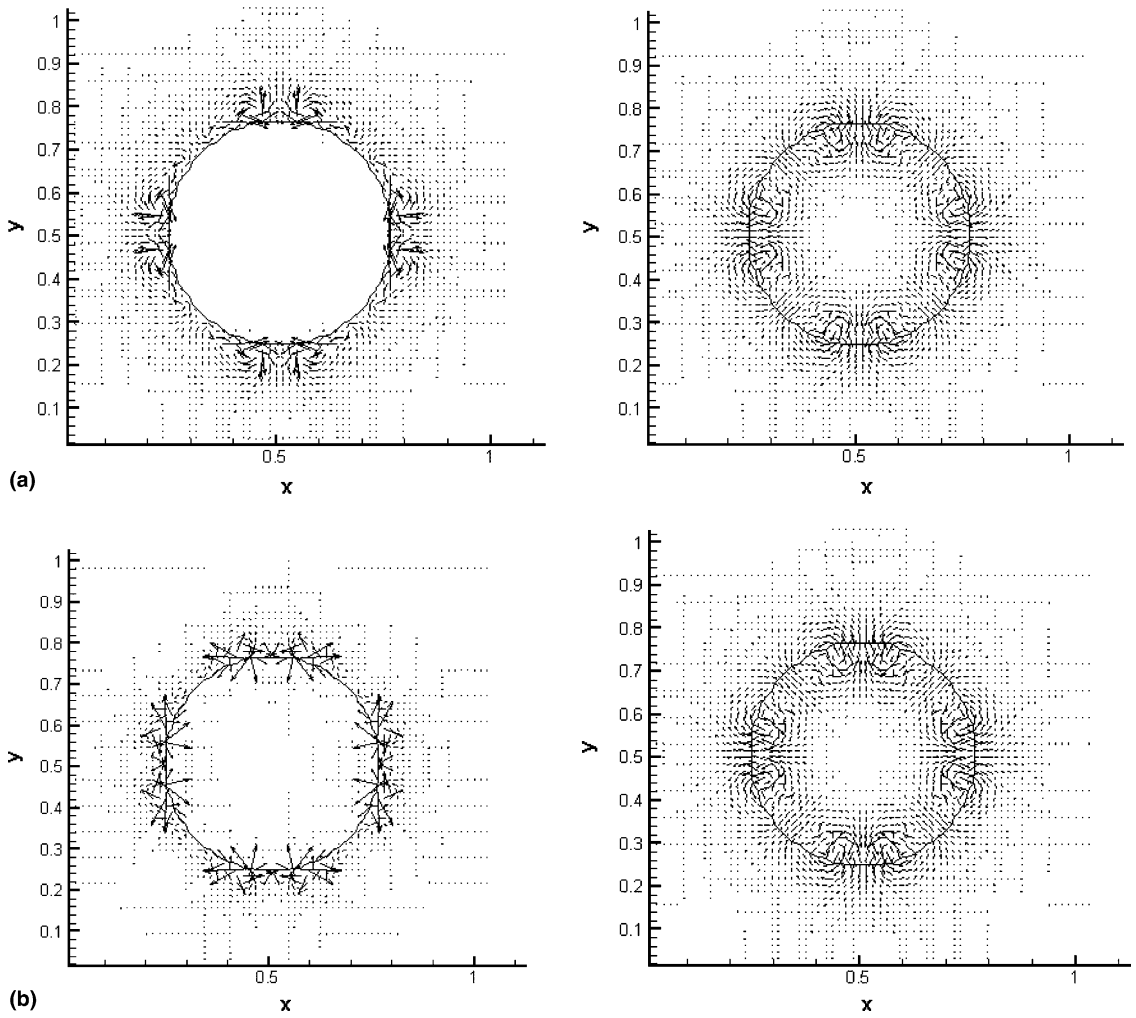


Fig. 9. Spurious currents (with different velocity scales) using CSF model (a) without and (b) with density modification. Figure on the left are without PCIL model and those on the right are with PCIL model.

$x$-direction and it is set equal to one. A $66 \times 66$ mesh and a time step of $10^{-5}$ is chosen for all of the calculations. This time step is determined based on conducting a series of computations to obtain independency of the solution to the time steps.

From the dimensional analysis, the above-mentioned physical properties are grouped into three non-dimensional parameters:

$$Oh_1 = \frac{\mu_1}{\sqrt{r\rho_1\sigma}}, \quad \frac{\rho_1}{\rho_2} \quad \text{and} \quad \frac{\mu_1}{\mu_2}, \tag{41}$$

where $Oh_1$ is Ohnesorge number based on the properties of fluid 1 contained in the drop. Following Popinet and Zaleski [26] and Scardovelli and Zaleski [33], for a drop with a constant radius and from the dimensional analysis, the velocity of the spurious currents is only a linear function of the surface tension

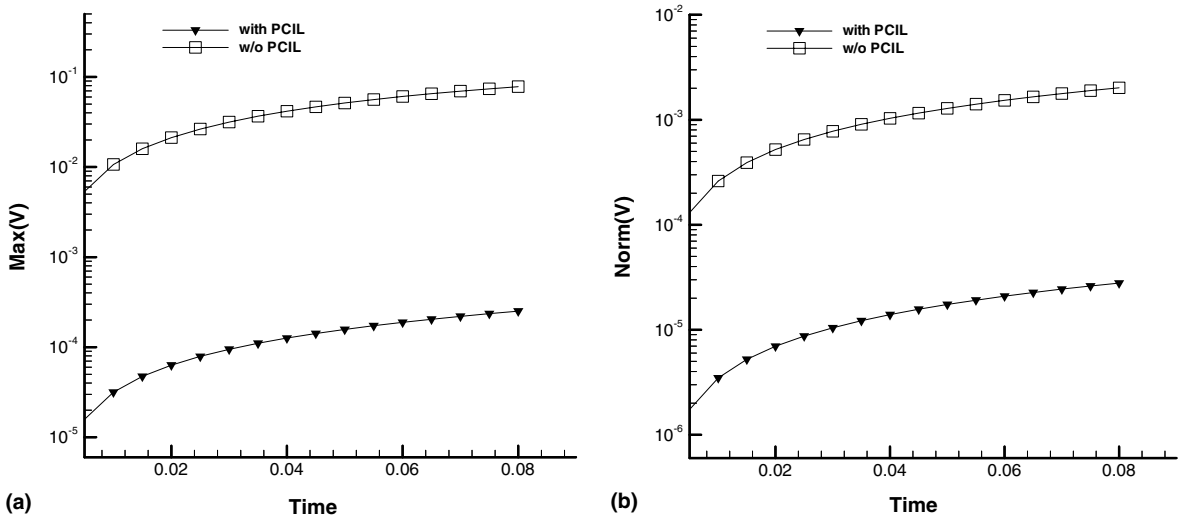


Fig. 10. (a) Maximum and (b) norm of spurious velocities using CSS model.

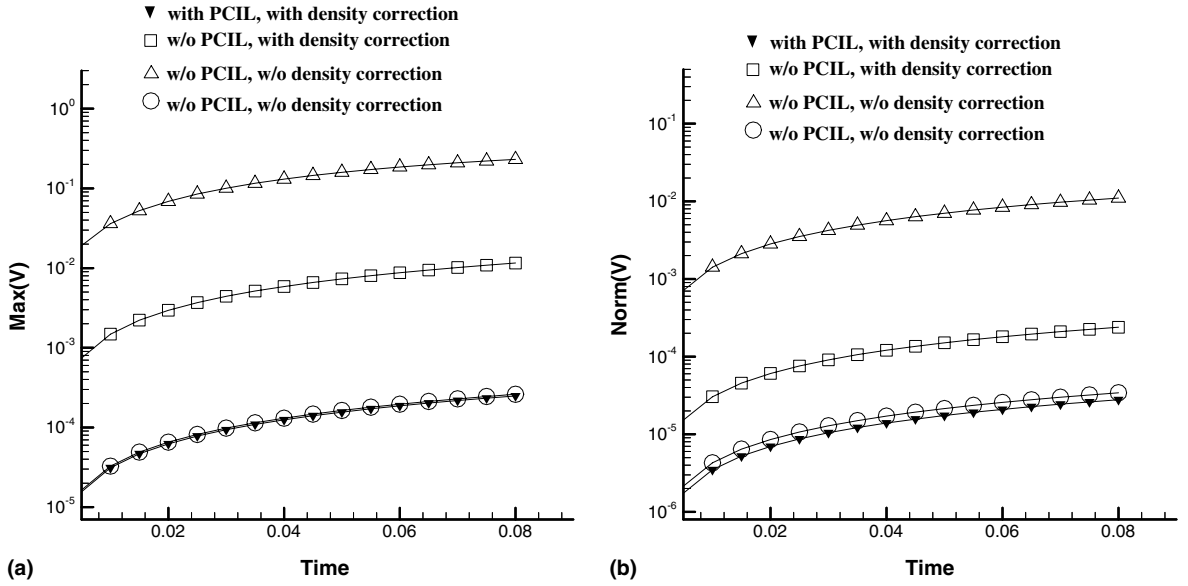


Fig. 11. (a) Maximum and (b) norm of spurious velocities using CSF model.

coefficient and viscosity, i.e., $u \sim \sigma/\mu$, and it is not a function of density. Thus it is expected that as the density of the fluid is changed, the velocity of the spurious currents remains constant.

A wide range of values including the properties of water (fluid 1) and air (fluid 2) are used for the above parameters. The results are presented in terms of the norms of the velocity (mean values of the absolute velocity) and the maximum values of the velocity of the spurious currents as a function of various variables.

Figs. 6 and 7 show the spurious currents for a water droplet in air (i.e., $\rho_1/\rho_2 = 830.545$, $\mu_1/\mu_2 = 54.945$). The Ohnesorge number based on the water properties ($Oh_1$) is $1.17 \times 10^{-4}$. In these cases, the number of

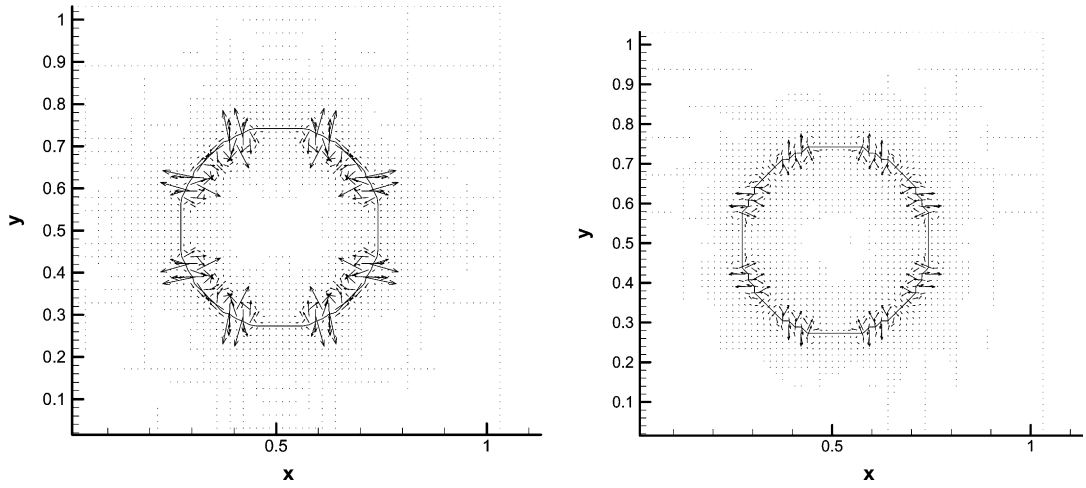


Fig. 12. Spurious currents (with different velocity scales) for a bubbles using CSS model. Figure on the right is without PCIL model, and one on the right is with PCIL model.

time steps, $N$, is 8000. The same scale for the velocity vectors is used in these figures. Fig. 6 shows the results using CSS, with and without the PCIL model. Addition of the PCIL model results in a much smaller spurious currents. The maximum and the norm velocities of the spurious currents for three time steps are given in Table 2. By using PCIL model, the maximum and the norm velocities of the spurious currents decrease by up to three orders of magnitude.

Fig. 7 shows the velocity vectors for the spurious currents at three different times using the CSF, with and without the PCIL model. We have compared the results with and without the density correction factor, the second fraction in Eq. (25). For these cases, the maximum and the norm velocities of the spurious currents at three different time steps are given in Tables 3 and 4, respectively. Figs. 8 and 9 are similar to those in Figs. 6 and 7, but each figure has a different velocity scale. These figures show that the flow structure of the spurious currents is different when the PCIL is used. With PCIL model, the magnitude of the spurious currents in both fluids are almost the same, whereas without the PCIL model, the spurious currents are dominant in the lighter fluid.

Figs. 10 and 11 show the velocities of the spurious currents as a function of time for the above six cases. As can be seen the velocities of spurious currents produced by both CSS and CSF models are reduced by orders of magnitudes when the PCIL model is used. In the CSF model, when the PCIL model and the density ratio correction are not used, the spurious currents are larger than that of the CSS model. Once the density correction ratio is added, the spurious currents become smaller, but they are still significant. By implementing the PCIL model the velocities of the spurious currents drop by about two orders of magnitude. Note that in all the cases studied, the spurious currents still tend to increase with time. From Fig. 7 and also from the third and the fifth columns of Tables 3 and 4, it can be seen that the implementation of the PCIL factor is enough to reduce the spurious currents and there is no need to implement the density ratio correction in addition to the PCIL. Therefore, the PCIL model is a better alternative to the density ratio correction, which is somewhat a heuristic relation and does not reduce the spurious currents as much as the PCIL model.

In order to show that there is symmetry in the PCIL method, and the method works for all cases regardless of where fluids one and two are located, we have repeated the calculations for a bubble inside a liquid (the inverse of a drop). The flow condition is similar to the drop case except that fluid one is replaced by fluid two and vice versa. The results for the spurious currents produced around the interface of the bubble,

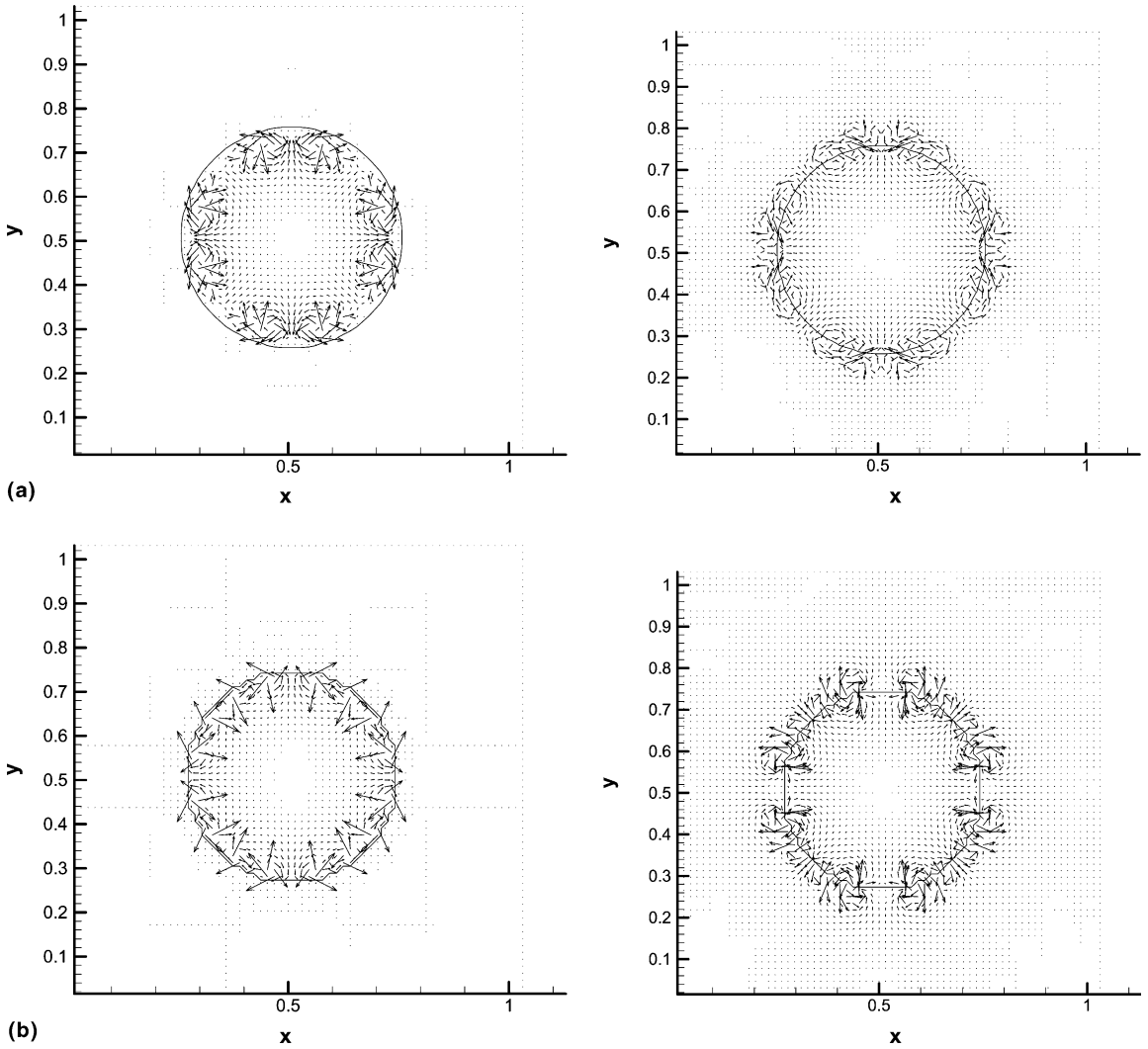


Fig. 13. Spurious currents (with different velocity scales) for a static bubble using CSF model. (a) Without and (b) with density modification. Figures on the left are without PCIL model and figures on the right are with PCIL model.

Table 5
Values of the maximum and the norm of the velocities of spurious currents for a bubble

| Case | CSS model | | CSF model w/o density correction | | CSF model with density correction | |
|---|---|---|---|---|---|---|
| | w/o PCIL | with PCIL | w/o PCIL | with PCIL | w/o PCIL | With PCIL |
| Maximum velocity | 5.063e − 1 | 8.604e − 3 | 2.046e − 1 | 3.934e − 4 | 8.647e − 2 | 3.345e − 4 |
| Norm velocity | 9.363e − 3 | 2.550e − 4 | 5.087e − 3 | 2.317e − 5 | 1.318e − 3 | 1.938e − 5 |

similar to that of Figs. 8 and 9, are shown in Figs. 12 and 13. In this case, as we expected, when the PCIL model is not used, the spurious currents are mainly inside of the bubble where the gas is located. But after we apply the PCIL model, the spurious currents are significantly reduced. The magnitude of the currents

inside and outside of the bubble is about the same. The magnitude of the maximum and the norm velocities of the spurious currents, at the time step of 8000, for the above-mentioned six cases, are given in Table 5. As can be seen, the velocities reduce by several orders of magnitude as we use the PCIL model. The rest of the results presented below are for a liquid drop.

Fig. 14 shows the relative error in calculation of pressure as a function of number of time steps for different cases. The relative error is defined as:

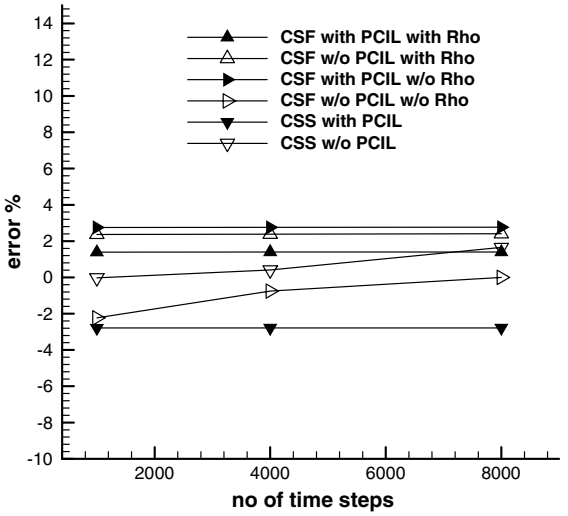


Fig. 14. Relative error in calculation of pressure at different times.

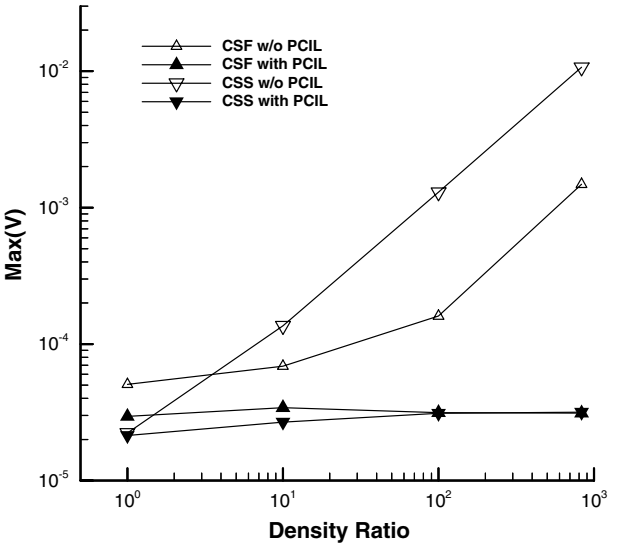


Fig. 15. Maximum spurious velocity as a function of density ratio.

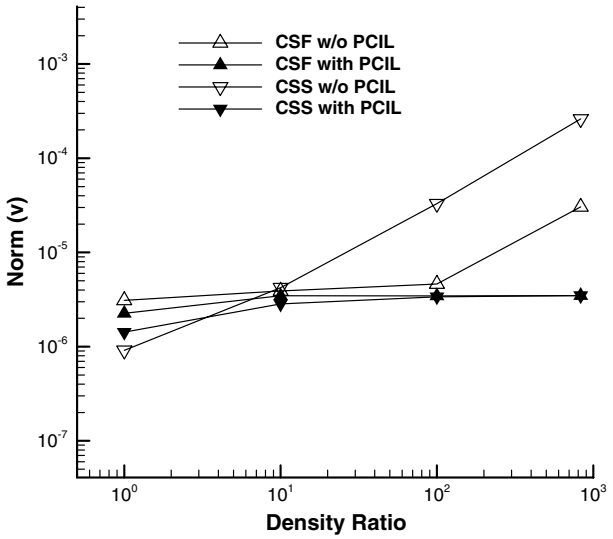


Fig. 16. Norm of spurious velocity as a function of density ratio.

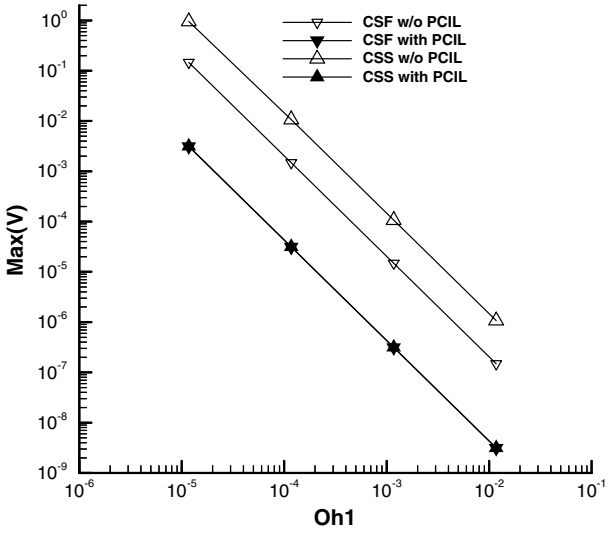


Fig. 17. Maximum spurious velocity as a function of Ohnesorge number.

$$error = \frac{(\overline{p_1} - \overline{p_2}) - \frac{\sigma}{R}}{\frac{\sigma}{R}}, \tag{42}$$

where $\overline{p_1}$ and $\overline{p_2}$ are the mean values of pressure inside and outside of the drop. Note that if the pressures $\overline{p_1}$ and $\overline{p_2}$ were calculated exactly, the value of the *error* would be zero. Fig. 14 shows that all six cases examined calculate the pressure rather accurately and the *error* is less than 3%.

Effects of fluid property ratios, namely, density and viscosity ratios, and the Ohnesorge number are considered here. Figs. 15 and 16 show the maximum and the norm velocities of the spurious currents as

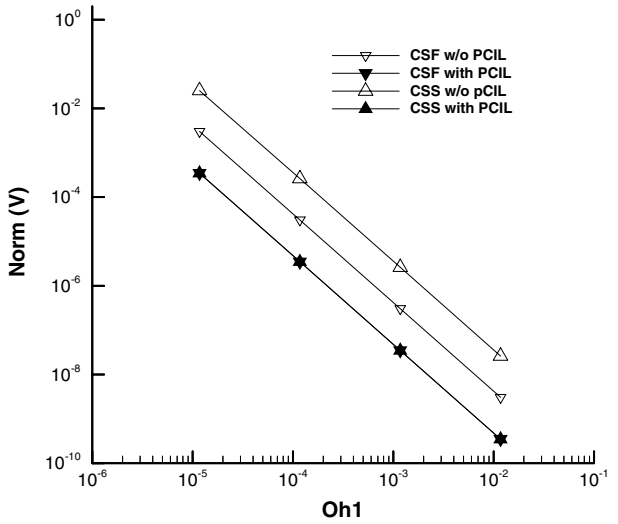


Fig. 18. Norm of spurious velocity as a function of Ohnesorge number.

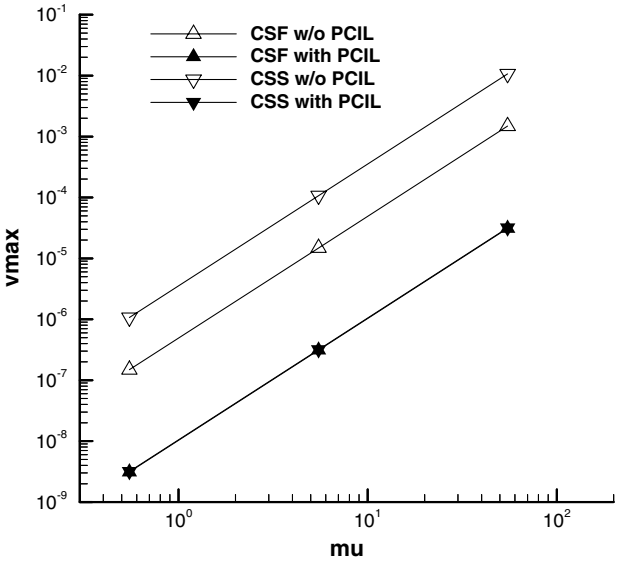


Fig. 19. Maximum spurious velocity as a function of viscosity ratio.

a function of density ratio for CSS and CSF models, respectively. Results for cases with and without the PCIL model are presented. The viscosity ratio ($\mu_1/\mu_2$) is 54.945 and $Oh_1 = 1.17 \times 10^{-4}$ (equivalent to that of a water drop in air). These figures show that as the density ratio increases, the velocity of the spurious currents remains constant when PCIL is used, while it increases when it is not used. This indicates that PCIL model is in agreement with the results of the dimensional analysis, namely, $u \sim \sigma/\mu$, which shows that velocity does not change with density. Figs. 15 and 16 show that PCIL model may be used to obtain reasonable results for high density ratios without generating extra spurious currents.

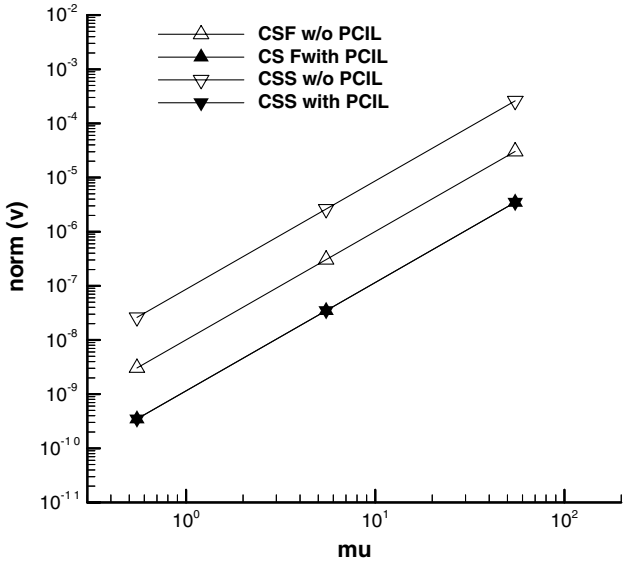


Fig. 20. Norm spurious velocity as a function of viscosity ratio.

Figs. 17 and 18 show the maximum and the norm velocities of the spurious currents as a function of the Ohnesorge number for the CSS and the CSF models. Results for both cases with and without the PCIL model are presented. In these figures, the density ratio ($\rho_1/\rho_2$) is 830.545 and the viscosity ratio ($\mu_1/\mu_2$) is 54.945. It is shown that the spurious velocities decrease by two orders of magnitude when the PCIL is used. As $Oh_1$ increases, the spurious velocities decrease by a power law. The variation of the velocity with $Oh_1$ is also in agreement with the dimensional analysis which indicates $u \sim \sigma/\mu$.

Figs. 19 and 20 show the maximum and the norm velocities of the spurious currents as a function of viscosity ratio for the CSS and the CSF models, respectively. Again, results for both cases with and without the PCIL model are presented. In these figures, the density ratio ($\rho_1/\rho_2$) is 830.545 and $Oh_1 = 1.17 \times 10^{-4}$. Here, $\mu_1$ has been changed and in order to keep $Oh_1$ constant, the surface tension coefficient is changed accordingly. It is shown that the spurious velocities decrease by more than two orders of magnitude when the correction is applied. As the viscosity ratio increases, the spurious velocities increase by a power law. This variation is also in agreement with the dimensional analysis which indicates that $u \sim \sigma/\mu$ [26,33].

## 6. Conclusions

A new method for the calculation of the pressure force at the interface cells for VOF based methods is presented. In this method, first the intersection locations of an interface with the interfacial cell faces are determined. The area of a cell face, which is in contact with the heavier fluid, is normalized with the cell face area to obtain a factor $H$. Then, the two values of $H$s obtained from the cells on both sides of each internal cell face are averaged. Finally, the capillary force used in the momentum equation is corrected by multiplying it by the factor $H$ determined for the cell faces. The new interface volumetric pressure force defined for each cell is then obtained from the following equation:

$$F^{\mathrm{st}} = H\sigma\kappa n\delta_S. \tag{43}$$

The new method is applied to modeling a drop and a bubble in a motionless fluid. It is shown that the velocities of the spurious currents decrease by more than two orders of magnitude. Variation of the velocity of

the spurious currents with Ohnesorge number, density and viscosity ratios of the two fluids involved, are examined. It is found that the variation with the Ohnesorge number and the viscosity ratio is a power law. Changes in the density ratio do not affect the corrected version. However, the spurious currents drastically increase with the density ratio when pressure force is not corrected. Although the spurious currents are reduced by several orders of magnitude when the corrected pressure force is used, there are still some currents in the flow. They increase with time at a rate similar to those in CSF and CSS methods but with much smaller magnitudes. These currents may be further reduced by using a more accurate calculation of normal vectors and the interface locations.

## Acknowledgments

Authors thank Prof. Stephane Zaleski for providing his SURFER code. Financial support from MMO is gratefully acknowledged.

## References

[1] C.W. Hirt, B.D. Nichols, Volume of Fluid (VOF) method for the dynamics of free boundaries, J. Comput. Phys. 39 (1981) 201–225.
[2] F.H. Harlow, J.E. Welch, Numerical calculation of time dependent viscous incompressible flow of fluid with free surface, Phys. Fluids 8 (1965) 2182–2189.
[3] W.F. Noh, P.R. Woodward, SLIC (Simple Line Interface Method), Lecture Notes Phys. 59 (1976).
[4] B.D. Nichols, W.C. Hirt, R.S. Hotchkiss, A Solution Algorithm for Transient Fluid Flow with Multiple Free Boundaries, Technical Report, La-8355, Los Alamos National Lab., 1980.
[5] A.J. Chorin, Flame advection and propagation algorithms, J. Comput. Phys. 35 (1980) 1–11.
[6] P.K. Barr, W.T. Ashurst, An Interface Scheme for Turbulent Flame Propagation, Technical Report SAND 82-7873, Sandia Nat. Lab. 1984.
[7] R. DeBar, Fundamentals of the KRAKEN code, Technical Report UCIR-760, Lawrence Livermore Nat. Lab., 1974.
[8] D.L. Youngs, Time-dependent multi-material flow with large fluid distribution, in: K.W. Morton, M.L. Norman (Eds.), Numerical Methods for Fluid Dynamics, 1986, pp. 187–221.
[9] N. Ashgriz, J.Y. Poo, FLAIR: Flux line-segment model for advection and interface reconstruction, J. Comput. Phys. 93 (1991) 449–468.
[10] L.F. Henderson, P. Colella, E.G. Puckett, On the refraction of shock waves at a slow-fast gas interface, J. Fluid Mech. 224 (1991) 1–27.
[11] E.G. Puckett, A.S. Almgren, J.B. Bell, D.L. Marcus, W.J. Rider, A high-order projection method for tracking fluid intrefaces in variable density incompressible flows, J. Comput. Phys. 130 (1997) 269–282.
[12] S.O. Kim, H.C. No, Second order model for free surface convection and interface reconstruction, Int. J. Numer. Methods Fluids 26 (1) (1998) 79.
[13] J.E. Pilliod, An analysis of piecewise linear interface reconstruction algorithm for volume of fluid methods, M.Sc. Thesis, Department of Mathematics, University of California, Davis, 1992.
[14] J.E. Pilliod, A second order unsplit method for modeling flames in two-dimensional compressible flow, Ph.D. Thesis, Department of Mathematics, University of California, Davis, 1996.
[15] W.J. Rider, D.B. Kothe, Reconstructing volume tracking, J. Comput. Phys. 141 (1998) 112.
[16] S.O. Unverdi, G. Tryggvason, A front tracking method for viscous, incompressible, multi-fluid flows, J. Comput. Phys. 32 (1992) 101–136.
[17] J.U. Brackbill, D.B. Kothe, C. Zemach, A continuum method for modeling surface tension, J. Comput. Phys. 100 (1992) 335–354.
[18] J.U. Brackbill, D.B. Kothe, Dynamic modeling of the surface tension, in: Proceedings of the 3rd Microgravity Fluid Physics Conference, Cleveland, OH, 1996, pp. 693–698.
[19] I. Aleinov, E.G. Puckett, Computing surface tension with high-order kernels, in: H.A. Dwyer (Ed.), Proceedings of the Sixth International Symposium on Computational Fluid dynamics, Lake Tahoe, NV, 1995, pp. 13–18.
[20] M. Bussmann, J. Mostaghimi, S. Chandra, On a three dimensional volume tracking model of droplet impact, Phys. Fluids 11 (1999) 1406–1417.
[21] J.J. Monaghan, Smoothed particle hydrodynamics, Ann. Rev. Astron. Astrophys. 30 (1992) 543–574.

[22] M.A. Rudman, A volume-tracking method for incompressible multifluid flows with large density variations, Int. J. Numer. Meth. Fluids 28 (1998) 357378.
[23] H.O. Nordmark, Rezoning for higher order vortex methods, J. Comput. Phys. 97 (1991) 366–397.
[24] C.S. Peskin, Numerical analysis of blood flow in the heart, J. Comput. Phys. 25 (1977) 220–252.
[25] B. Lafaurie, C. Nardone, R. Scardovelli, S. Zaleski, G. Zanetti, Modelling merging and fragmentation in multiphase flows with SURFER, J. Comput. Phys. 113 (1994) 134–147.
[26] S. Popinet, S. Zaleski, A front-tracking algorithm for accurate representation of surface tension, Int. J. Numer. Meth. Fluids 30 (1999) 775793.
[27] M. Meier, H. Yadigaroglu, B.L. Smith, A novel technique for including surface tension in PLIC-VOF methods, Eur. J. Mech. B/Fluids 21 (2002) 6173.
[28] Y. Renardy, M. Renardy, PROST: A parabolic reconstruction of surface tension for the volume-of-fluid method, J. Comput. Phys. 183 (2002) 400–421.
[29] D. Jamet, D. Torres, J.U. Brackbill, On the theory and computation of surface tension: the elimination of parasitic currents through energy conservation in the second-gradient method, J. Comput. Phys. 182 (2002) 262–276.
[30] D.B. Kothe, W.J. Rider, S.J. Mosso, J.S. Brock, Volume tracking of interfaces having surface tension in two and three dimensions, AIAA 96-0859, 1996.
[31] S. Zaleski, J. Li, S. Succi, Two-dimensional Navier–Stokes simulation of deformation and break-up of liquid patches, Phys. Rev. Lett. 75 (1995) 244.
[32] S. Zaleski, Simulation of high Reynolds number breakup of liquid–gas interface, Lecture series, von Karman Institute for Fluid Dynamics, 1996.
[33] R. Scardovelli, S. Zaleski, Direct numerical simulation of free surface and interfacial flow, Annu. Rev. Fluid Mech. 31 (1999) 567–603.